Circular RNA, CDR1as, modulates spinal fibrosis via the miR-7a-5p/TGF-βR2 axis and the Smads signaling pathway

Wenzhao Wang (wayne1898@163.com)
Sichuan University https://orcid.org/0000-0001-5106-4862
Dong He
Shandong University
Peijia Zhu
Sichuan University
Kaiwen Liu
Shandong University
Shaoyi Wang
Shandong University
Qiyu Bo
Shandong University
Jianlu Wei
Shandong University https://orcid.org/0000-0003-3166-5227

Research Article

Keywords: spinal cord injury, fibrosis, CircRNA, CDR1as, miR-7

Posted Date: March 15th, 2021

DOI: https://doi.org/10.21203/rs.3.rs-187464/v1

Abstract

Damage to the spinal cord is the most serious complication of spinal injury. The method to reduce fibrogenesis after spinal cord injury, to facilitate repair, is an ongoing hurdle despite advancements in research. Non-coding RNA plays an important role in the progression of many diseases, but the study of its role in the progression of spinal fibrosis is still emerging. Here, we investigated the function of circular RNAs, specifically CDR1as, in spinal fibrosis and characterized its molecular mechanism and pathophysiology. The presence of CDR1as in the spinal cord was verified by sequencing and polymerase chain reaction assays. Further, gene and protein expression of miR-7a-5p and TGF-βR2 were measured to evaluate their predicted interactions. The combination miR-7a-5p/TGF-βR2 was predicted by bioinformatics and validated using a luciferase reporter assay. The regulatory effects and activation pathways of miR-7a-5p and CDR1as on spinal fibrosis were subsequently verified by Western blot. miR-7a-5p inhibitor and siCDR1as were transfected and inhibited the effect of siCDR1as. These results indicate that CDR1as/miR-7a-5p/TGF-βR2 interactions may exert important functions and suggest potential therapeutic targets for treating spinal fibrotic diseases.

Introduction

Over 4,500 years ago, military physicians recognized that a crushed or transected spinal cord could not regenerate; today, despite a long history of conceptual advances, the goal of practical, reproducible, functionally meaningful, and clinically translational spinal cord regeneration has yet to be achieved [1]. War injuries, car accidents, and falls all contribute to the incidence of spinal cord injury SCI [2, 3]. Worryingly, as the population ages, the number of recorded cases of traumatic SCIs due to falls has risen from 16 to 30.5% since 2012 [1].The clinical presentation of SCI depends on the severity and location of the injury. Currently, most acute treatments are aimed at stabilizing the spinal cord and restoring homeostasis, while long-term treatments mainly manage the symptoms of maladaptive and secondary complications [3, 4]. Regardless of etiology, severity, or complexity, spinal cord injuries exhibit three lesion sites: the non-nerve (interstitial) lesion core, the scar, and the reactive surviving nerve tissue. The compartments are made up of very different cell types that have completely different roles in repair and regeneration [1, 5]. The particular cellular biology and molecular mechanisms in each chamber affect axon growth or regeneration in different ways. Understanding these differences is critical to understanding the requirements to achieve or improve regeneration and to design rational, mechanistically targeted interventions [2, 3, 6]. Based on the theory that an injured axon cannot grow beyond obstructive glial and connective tissue, it is widely believed that after central nervous system injury, scars will form and axonal regeneration will be blocked [7, 8]. Fibroblasts are the main connective tissue cells in the body, and these cells provide the structural framework throughout the extracellular matrix and only invade or occur in the central nervous system after injury [9-11].

Circular RNAs (circRNAs) are a class of primitive non-coding RNA (ncRNAs) that were first discovered by electron microscopy in the late 1970s, in human cell lines [12, 13]. Initially, these circRNAs were considered to be potentially pathogenic by-products of abnormal splicing or "transcription/splicing noise",

and thus they received little attention. However, with the development and improvement of transcriptomics and bioinformatics, doubts about the existence and significance of circRNAs have gradually disappeared [14]. Unlike linear RNAs, circRNAs are characterized by a remarkable continuous closed-loop structure, formed by a “back-splicing” event wherein a covalent bond is formed between the splice donor and the splice acceptor [13]. This unique loop structure prevents circRNAs from exhibiting typical mRNA-processing characteristics, such as a poly(A)-tail, which makes them structurally stable and highly resistant to exonuclease degradation [15]. circRNAs have been reported to act as microRNA(miRNA) sponges to competitively modulate miRNA expression levels and interact with RNA-binding proteins (RBPs) and regulate post-transcriptional gene expression, thereby suppressing miRNA function, [14]. Most strikingly, circRNA expression is associated with the occurrence and development of many diseases, including a variety of cancers, endocrinium, cardiovascular disease, skeletal musculature disease, and neurological diseases [15]. However, whether circRNAs play a regulatory role in scar formation after SCI has rarely been reported. As such, there is a need to identify differentially expressed circRNAs and to clarify their general mechanism in spinal fibrosis.

CDR1as, also called CiRS-7 and circRNA0001878, is one of the earliest discovered and most studied circRNAs [7]. CDR1as and sponging miR-7a-5p have been associated with nervous system development, repair, and diseases [13]. In a previous study, we employed SCI mouse models and performed high-throughput sequencing of the tissue within the lesion epicenter during the acute phase [16]. In the present study, we analyzed the sequencing data and found that both CDR1as and miR-7a-5p were significant differentially expressed after SCI. Whether CDR1as/miR-7a-5p interactions have functional effects on spinal fibrosis remains to be determined. To this end, we constructed a CDR1as/miR-7a-5p /TGF-βR2 targeted regulatory network, based on the sequencing results. Using Kyoto Encyclopedia of Genes and Genomes (KEGG) analysis, we looked for potential functional downstream pathway cascade chain proteins. Furthermore, we tracked the changes of miR-7a-5p and TGF-βR2 expression of the interacting axis *in vivo* within 14 days of SCI, and then verified the regulatory axis and downstream pathways through *in vitro* experiments. This study adds knowledge to the repertoire of ncRNAs activity during the pathophysiological process of SCI, and provides novel insight for future therapeutic strategies for spinal fibrosis.

Materials And Methods

Genome Mapping, KEGG Pathways, and ncRNA Regulatory Network Analysis

The sequencing data of SCI tissues were derived from previous studies [16], The samples were divided into an SCI group and a Sham group, with three replicates each. The tissue samples were derived from the spinal lesion epicenter of modified standard Allen’s drop mouse model, 3 days after SCI. Sample reads were aligned to the reference genome from Ensembl or National Center for Biotechnology Information databases using the Tophat 2 [17] package, which initially removed a portion of the reads based on the quality control information accompanying each read and then mapped the reads to the reference genome. Tophat allows multiple alignments per read, builds a database of potential splice

junctions, and compares the previously unmapped reads against a database of putative junctions. The aligned read files were processed by in-house scripts, which use the normalized RNA-seq fragment counts to measure the relative abundances of the transcripts. The unit of measurement is fragment per kilobase of exon model per million (FPKM) reads mapped. CIRCExplorer was used for denovo assembly of the mapped reads to circRNAs [18]. The assembled circRNAs from all samples were used to identify unique circRNAs; circRNAs were identified if they had a statistical p-value of < 0.05.

For pathway significance-enrichment analysis, we used a major public database, KEGG (https://www.kegg.jp/) [19]. To determine the most important biochemical, metabolic, and signal transduction pathways, a hypergeometric test was applied to isolate the significantly enriched pathways involving genes that were differentially expressed, compared with the whole-genome background.

An ncRNA regulatory network was constructed to profile the interactions and functional links among dysregulated messenger RNAs (mRNAs), miRNAs, and circRNAs in the acute stage of SCI. The targets of miRNAs were predicted by TargetScan (http://www.targetscan.org/) by adopting the default parameters, as previously described [20]. CircRNA/miRNA/mRNA interaction networks were constructed using Cytoscape (San Diego, CA, USA).

Construction of mouse SCI model

Eighteen (nine for the SCI group and nine for the Sham group), healthy, male C57BL/6 mice were used for our animal models, following a previously used approach [16]. In brief, in the SCI group, the exposed spinal cord was struck using a 6 g weight, which was dropped from a height of 6 cm (Allen's drop). The sham group had the T8–T10 segments of the thoracic vertebra exposed without an Allen's drop. At each experimental time point (3, 7, and 14 days after surgery), three mice from each group were randomly selected. Tissue was then extracted for quantitative reverse-transcription PCR (qRT-PCR) and Western Blot.

Primary cell extraction, Culture, Cytological identification and Transfection

Tissue from twenty C57BL/6 mice was used for primary spinal fibroblast extraction within 3 days of birth. After the isolated spinal cord was cut into pieces, 0.125% trypsin of 10 times volume was added and digested for 15 min in a magnetic mixer at 37℃. Medium was added for neutralization and the mixture was centrifuged at 1,000rpm for 5 min; then, the supernatant was discarded. The pellet was cultured in t-25 culture bottles, placed in an incubator at 37℃ with 5% CO_2, and cultured in modified Eagle's medium (Life Technologies, Carlsbad, CA, USA) containing 10 % fetal bovine serum (Gibco, Brisbane, Australia) and 100 IU/mL penicillin–streptomycin (Gibco). The medium was renewed after 24 hours. The cell density reached about 90% after a week of continuous cell culture. The cells were digested normally with 0.25% trypsin, placed in an incubator for 30-40 min after placing the culture flasks back inside the incubator, the culture medium was aspirated, and the non-adhered cells were discarded. Newly made culture medium was added and the cells were placed in an incubator at 37℃ with 5% CO2. The medium was changed 2-3 days later. Fibroblasts were identified by immunofluorescence, as previously

described [20]. In brief, after washing, permeating, and blocking, cells were incubated with Type I collagen antibody (Abcam, Cambridge, UK) at 4℃, overnight. After incubating with a secondary antibody (Invitrogen, CA, USA) and staining with 4',6-diamidino-2-phenylindole (DAPI; Invitrogen), immunofluorescence was analyzed under a fluorescence microscope (Olympus Corporation, Tokyo, Japan). Transfection of siRNA-CDR1as (siB2009231003539885, RiboBio, Guangzhou, China, GCCGTATCCAGGGTTTCCA), miR-7a-5p mimics, miR-7a-5p inhibitor, and their negative controls (RiboBio) was initiated when the cells were 30%–50% confluent. After 48 hours, the cells were stimulated with TGF-β (10 ng/ml, ACRO, Beijing, China) for 48 h.

RNA preparation and PCR validation

All qRT-PCR assays were carried out as previously described [20]. In brief, total RNA was isolated and then verified/quantified by the OD260/280 absorbance ratio, then reverse-transcribed into cDNA. qRT-PCR was performed using the Applied Biosystems (Wilmington, DE, USA) 7500 RT-PCR system and repeated three times. GAPDH was used as an internal control to normalize relative circRNA and mRNA expression levels. miRNA expression levels were normalized by U6. The $2^{-\Delta\Delta CT}$ method was used for comparative quantitation. The specific primers used for each target were as follows: mmu-CDR1as-Forward: AATCTATGCCTTCCACAAATG; mmu-CDR1as-Reverse: GACCTTGACAGTGTTGGA; mmu-miR-7a-5p-Forward: TGGCGGTGGAAGACTAGTGAT; mmu-miR-7a-5p Reverse: TGTCGTATCCAGTGCAGGGTCCGAGGTATTCGCACTGGATACGACACAACA; TGF-βR2-Forward: CATCGCTCATCTCCACAGT; TGF-βR2-Reverse: ACACAGGCAACAGGTCAA; GAPDH-Forward: GTGGTGAAGCAGGCATCT; GAPDH-Reverse: GGTGGAAGAGTGGGAGTTG; U6-Forward: CTCGCTTCGGCAGCACA; U6-Reverse: AACGCTTCACGAATTTGCGT.

Reverse-transcriptase polymerase chain reactions (RT-PCR) were carried out in accordance with according to the manufacturer's instructions found in the Select RT kit (RiboBio, Guangzhou, China) The cDNA amplification reactions were performed with 2× Taq plus RTase Mix (RiboBio) and RT primer(C)*(10μM). PCR products were separated by electrophoresis on an agarose gel (1.5%) at 120 V of constant pressure for 30 min. Finally, Sanger sequencing (m-CDR1as-DP-219bp-R1) was performed. The specific primers for Sanger sequencing and RT-PCR were as follows: mmu-CDR1as-DP-219bp-Forward 1: GTGTATCGGCGTTTTGACATTC; mmu-CDR1as-DP-219bp-Reverse 1: ACTGAATTTACTGGAAGACTCTGAG; mmu-CDR1as-CP-201bp-Forward 2: TCCACATCTTCCCAAAATCCA; mmu-CDR1as-CP-201bp-Reverse 2: GAATGTCAAAACGCCGATACAC.

Protein isolation and Western blot

Total proteins were extracted then separated by electrophoresis on sodium dodecyl sulphate-polyacrylamide gels (Solarbio, Beijing, China) and subsequently transferred to 0.22-mm polyvinylidene difluoride membranes (Solarbio). The membranes were blocked with 5% skim milk at room temperature for 1 hour. Then, the membranes were incubated with primary antibodies overnight at 4℃. Incubation with secondary antibodies (Solarbio) was performed the following day for 2 hours at room temperature. The antibodies (anti-Fibronectin, anti-Smad7, anti-p-Smad2, anti-p-Smad3, anti-Smad2/3, and anti-

GAPDH antibody) used in this study were formulated as previously described [20, 21]. The protein levels were visualized using the West Pico ECL Substrate (Solarbio), and GAPDH was used as an endogenous control for normalization.

Luciferase reporter assay and fluorescence in situ hybridization

293T cells were inoculated into 96-well plates at a confluence of 70%. The plasmids pMIR-REPORT-CDR1as (WT) (LC Science, Houston, TX) and pMIR-REPORT-CDR1as (MT1+MT2) (LC Science) were transfected 24 hours later. 0.2g concentration of transfection reagent was used, the final concentration of microRNA was 100 nM. The DNA, miRNA, transfection reagent, and incubate were diluted and set at room temperature for 5 minutes. The diluted DNA and miRNA were mixed with the transfection reagent (Invitrogen), respectively, and incubated at room temperature for 20 minutes. Approximately 50 μL of culture medium was discarded from each well and 25 μL DNA transfection mixture and 25μL miRNA transfection mixture were added to each well. Data were measured after 2S. Following the addition of 50μL of pre-mixed Stop&Glo reagent to each well. Fluorescence was detected using the Opera Phenix HCS system (PerkinElmer, MA, USA).

Statistical Analysis

Statistical analyses were carried out using GraphPad Prism software, and data are expressed as mean ± standard deviation (SD). Statistical significance between the two groups was assessed using independent-samples t-test, while analysis of variance (ANOVA) with post-hoc Dunnett's corrections was performed for comparison between two or more groups. $P < 0.05$ was considered statistically significant.

Results

Identification and Validation of CDR1as expression

Information and chromosomal distribution of the differentially expressed circRNAs, Our analysis revealed that CDR1as is down-regulated after SCI, compared with the Sham group (log2 fold-change = -1.61, p 0.05; Figure 1 A-B). CDR1as is transcribed from the antisense strand of the CDR1as gene (ChX:61173982–61195535) (Figure 1C). CircRNAs are single-stranded, closed-loop RNAs, generally formed by transcribed linear RNA through back-splicing processing. Due to the diversified variable shearing during RNA processing, it is often necessary to identify circRNAs by high-throughput sequencing and bioinformatics analysis, including the identification of splice junctions and the identification of circRNA sequence composition. Forward Primer-1 and Reverse Primer-1 can be combined for PCR to detect the conventional circRNA expression levels and subsequent sequencing of the amplified product can identify the exact sequence of splice junction. The splice junction sites of CDR1as were validated by Sanger sequencing (Figure 1D). We designed two sets of primers for CDR1as, to verify the head-to-tail splicing of CDR1as. cDNA and genomic DNA(gDNA) amplified results of CDR1as (divergent) and linear transcripts (convergent) primers were compared. However, the divergent primers could only amplify CDR1as using cDNA as templates, and no amplification product was observed on using gDNA (Figure 1E). The expression of CDR1as in the lesion epicenter decreased significantly within 3 days after SCI

compared with the level of expression in the Sham group, as evidenced by qRT-PCR, (Figure 1F), **p < 0.01.

Prediction of CDR1as/miR-7a-5p/TGF-βR2 network and the downstream Smads signaling pathways

After interaction network analysis, we obtained the predicted targeted binding relationship results of all the differentially expressed circRNAs. due to the space constraints, we only selected CDR1as and six other randomly selected differentially expressed circRNAs (ciRNA948, circRNA14958, circRNA002087, circRNA0005489, circRNA722, and circRNA14885) (Figure S1). CDR1as/miR-7a-5p/TGF-βR2 is marked with a red-dotted line in the partial plot of the interaction network (Figure 2). KEGG signaling pathway analysis showed that the TGF-β/Smads signaling pathway-related proteins were significantly differentially expressed after SCI. Stringtie enrichment analysis was carried out, showing that there are complex regulatory relationships among the pathway-related proteins. The key proteins are highlighted in red (Figure 3).

Construction and confirmation of miR-7a-5p/TGF-βR2 paired relationship

The relative expression of miR-7a-5p was measured by qRT-PCR on days 3,7, and 14 post-SCI and compared with the expression levels in the sham group. The expression of miR-7a-5p decreased significantly 3 days after SCI, and then increased slightly until day 7 post-SCI, then increased slowly until 14 days after SCI. However, expression levels could only recover to one-third of the expression in the sham group on day 14 post-SCI (Figure 4A). The relative expression of TGF-βR2 was also measured by qRT-PCR and revealed that TGF-βR2 expression was significantly higher than that of the Sham group, 3 days after SCI. The level reached its peak at day 7 post-SCI, although the expression level on day 14 was lower than that on day 7. However, expression was still significantly higher than that of the sham group (Figure 4B). miR-7a-5p/TGF-βR2 axis was predicted and constructed using TargetScan (Figure 4C). The miR-135b-5p specific target site in the 3'UTR of TGF-βR2 was predicted as GTCTTCC and the binding sites were verified by fluorescent reporters (Figure 4D). The expression of TGF-βR2 protein was measured by Western Blot and revealed that the trend of protein expression was consistent with that of RNA (Figure 4E). **P<0.01, ***P<0.001.

CDR1as/miR-7a-5p/TGF-βR2 axis regulated the spinal fibroblast fibrosis

Immunofluorescence staining of Collagen I was used to verify primary spinal fibroblasts. Type I collagen in the cytoplasm of fibroblasts fluoresces green and the nucleus fluoresces blue after DAPI staining. After merging, the overlap of the cytoplasm and nucleus of the fibroblasts could be clearly seen, confirming that the extracted primary fibroblasts were pure and that there was no contamination with other cell types (Figure 5A-B). The expression levels of fibrosis-associated proteins, fibronectin and collagen I, were measured by Western Blot after treatment with miR-7a-5p mimics and siCDR1as with or without TGF-β1 transfection, respectively. The results showed that miR-7a-5p mimics significantly suppressed the expression of fibronectin and collagen I (Figure 7C). siCDR1as also effectively inhibited the expression of the fibrosis-associated proteins (Figure 5D). After the co-transfection of miR-7a-5p inhibitor and siCDR1as

in primary spinal fibroblasts, the results of the Western Blot showed that the effect of miR-7a-5p inhibitor and siCDR1as on fibrosis had an antagonistic effect, and the use of siCDR1as followed by the use of miR-7a-5p inhibitor weakened the effect of siCDR1as (Figure 5E).

CDR1as/miR-7a-5p/TGF-βR2 axis regulated the activation of Smads signaling pathway

The effects of miR-7a-5p mimics on Smads signaling were detected in primary spinal fibroblasts treated with or without TGF-β1, and the expression of TGF-βR2 were detected by Western blot. Additionally, we assessed the activity of the downstream protein Smad2/3 and phosphorylated-Smad2/3. The results of Western Blot showed that miR-7a-5p mimics inhibited the expression of TGF-βR2. Total expression levels of Smad2 and Smad3 were unchanged; however, the expression of phosphorylated Smad2 and Smad3 were inhibited. This confirmed that miR-7a-5p mimics inhibited the phosphorylation of Smad2 and Smad3 (Figure 6A). Simultaneously, functional effects of siCDR1as were verified. SiCDR1as had the same effect as miR-7a-5p mimics on the phosphorylation levels of Smad2 and Smad3 (Figure 6B). The results of Western Blot showed that co-transfection of the miR-7a-5p inhibitor and siCDR1as attenuated the effect of siCDR1as on inhibiting the Smad pathway (Figure 5E). Overall, the results indicated that CDR1as promotes fibrosis through the miR-7a-5p/TGF-βR2 axis via activating the Smads signaling pathway.

Discussion

Damage to the spinal cord is the most serious complication of spinal injury, and recovery of neurological function or motor function after SCI is a worldwide problem [1]. Studies have shown that axonal regeneration after SCI is the basis of nerve-cell repair and the key to functional recovery. The main obstacle of axonal regeneration is closely related to factors such as scar formation and the weakened intrinsic regeneration power of neurons. After SCI, it is common to see fibrous scarring and glial scar formation. These scars appear at different time points and fuse into a scar mass at about 2 weeks after injury. The inner layer is a dense fibrous scar and the outer layer is a glial scar, and the entire scar structure is known as the non-neural lesion core [6, 8] .The traditional thought is that the glial scar inhibits the axon regeneration process, and previous research from our lab as well others, has confirmed that the glial scar occurs gradually during a certain period of the recovery process. The site of the axon regeneration and connection plays an important role, while fibrous scarring causes a hypertrophic physical barrier to form. The secretion of NG2 proteoglycan molecules inhibits the formation of a chemical barrier after prolonged SCI periods, thus playing a role in inhibition, severely hampering functional axon regeneration and neural recovery[9, 11, 22].

miRNA are evolutionary conserved, 18-22-nt long noncoding RNAs [23]. miRNA has diverse targets in different organisms, and there are many complementary sequences that can interact with various proteins [24]. The function of miRNAs are regulated by many factors, among which circRNAs act as a kind of sponge to efficiently target and alter the activity of microRNAs. Thus, they have an important influence on the activity and function on miRNAs [15]. CircRNAs are a class of covalently bonded non-

coding RNA molecules with a loop structure[12]. They are structurally stable, functionally diverse, widely distributed, and are significantly expressed in the central nervous system, regulated the storage, sorting, and localization of miRNAs, also act as competitive RNAs for miRNAs in neurite growth and neuron migration [25]. One of the earliest discovered and most well-known circRNA is CDR1as, also termed ciRS-7(functions as miR-7 sponge) or circRNA0001878(circBase)[26]. For example, CDR1as was first discovered because of its bonding relationship with miR-671 as CDR1as contains a binding site for miR-671. This complementary combination induced Argonaute (AGO)-mediated cleavage of CDR1as. However, if none of the miR-7a-5p binding sites for CDR1as are complementary, for more than 12 nucleotides, AGO-mediated cleavage upon miR-7a-5p binding does not occur [27-29]. Interestingly, CDR1as harbors more than 70 conventional binding sites for miR-7 [30]. miR-7a-5p is found in zebrafish, drosophila melanogaster, mouse, rat, and human, suggesting that it has conserved stability across species. Interestingly, miR-7a-5p is transcribed from three loci in the human genome and one locus in the mouse genome [31]. miR-7-targeted transcripts, such as α-synuclein EGFR, RAF1, KLF4, PARP, SP1, and PI3K, play a regulatory role in pathophysiological processes of miR-7, such as in nerve development, nerve injury, central nervous system tumors, and Parkinson's disease [32]. Although some studies have demonstrated that the CDR1as/miR-7a-5p axis plays a potential regulatory role in various systems [33], there have been no studies on the potential role of CDR1as-mediated fibrosis in spinal fibroblasts.

Our previous RNA-sequencing results showed that CDR1as was significantly down-regulated in the lesion epicenter of the spinal cord. In this study, we first verified the existence of CDR1as in spinal cord tissue, and then used qRT-PCR to prove that the change of CDR1as expression after SCI was consistent with the sequencing results. Next, we constructed a differential expression interaction network based on the sequencing results. We predict the existence of a CDR1as/miR-7a-5p/TGF-βR2 interaction axis. We chose this interaction axis is not only due to the large differences in the expression of interaction axis members before and after SCI, but also based on previous research. We have previously confirmed that TGF-β initiates the process of fibrosis [21]. We have also successfully used miR-21 to attenuate the phosphorylation of Smads proteins downstream of TGF-βR1/2 [20]. However, the function of miR-21 is to promote the progression of fibrosis, so in this study, miR-7a-5p, which can competitively bind TGF-βR2, was taken into consideration. TGFBR2 has been involved in various diseases associated with fibrosis, and studies suggest that its inhibition could reduce the levels of p-Smad2/3 and thereby suppress fibrosis [7]. We performed KEGG analysis on the sequencing results and found that activation of the Smads pathway was changed differently before and after injury. Furthermore, we conducted enrichment analysis on this pathway and confirmed that there were numerous links between downstream proteins. After validation of the targeted relationship, the functions and pathways of CDR1as/miR-7a-5p/TGF-βR2 were included in the scope of validation. In vitro experiments were done to mimic the conditions observed in in the acute stage of injury, and TGF-β1-stimulated fibroblasts were used to simulate the physiological state after SCI [21]. miR-7a-5p mimic and siCDR1as were further used separately to stimulate the activated fibroblasts. Consistent with our prediction, both of them had inhibitory effects on fibrosis. When we co-transfected miR-7a-5p inhibitor with siCDR1as, the effect of siCDR1as was inhibited. These results confirmed the role of the CDR1as/miR-7a-5P/TGF- βR2 as a regulatory axis.

However, the present study has some limitations. Since there are one-to-many and many-to-one relationships between circRNAs and miRNAs, the targeted binding relationships verified in this study may not be unique. Because of the long sequences of circRNAs, a single circRNA can simultaneously combine with multiple miRNAs. For example, circHIPK3 can simultaneously bind nine miRNAs, including miRNA-152 and miRNA-193a [34]. It has been previously reported that CDR1as itself can also sponge miR-135 and inhibit its function [35]. Similarly, a miRNA can target multiple mRNAs simultaneously [14, 36]. For example, KLF4, which plays an important role in the neural repair process, can also be targeted and regulated by miR-7a-5p [37].The regulation process of ncRNAs may be a network rather than a single thread. Multiple miRNAs are bound by the same circRNA, and multiple targeted mRNAs are combined with the same miRNA. These interactions form a network, which may have synergistic or antagonistic effects through multiple pathways. In the future, we will screen, and verify, the downstream regulatory networks more accurately and fully elucidate the targeted interactions by combining a variety of circRNAs and miRNA mimics or inhibitors. In conclusion, the present study verified the structure and function of the CDR1as/miR-7a-5p/TGF-βR2 interaction axis in spinal fibrosis. Over-expression of miR-7a-5p could inhibit fibrosis by targeting TGF-βR2. siCDR1as was found to have the same effect as miR-7a-5p mimics and acted as an inhibitor of fibrosis molecules, through sponging miR-7a-5p. These findings provide new insight for the treatment of movement disorders caused by fibrosis after SCI.

Declarations

Acknowledgments

This work was supported partly by National Natural Science Foundation of China (81900804), and Shandong Provence Natural Science Foundation (ZR2019BH071). Sichuan Science and Technology Programs (NO. 2020JDRC0054) and China Postdoctoral Science Foundation Grant(2019M651064).

Funding: This work was supported partly by National Natural Science Foundation of China (81900804), and Shandong Provence Natural Science Foundation (ZR2019BH071). Sichuan Science and Technology Programs (NO. 2020JDRC0054) and China Postdoctoral Science Foundation Grant(2019M651064).

Conflicts of interest/Competing interests:

The authors declare no conflict of interests.

Ethics approval: All experimental procedures were approved by the Institutional Animal Care and Use Committee of Shandong University

Availability of data and material:

The data that support the findings of this study are available from the corresponding

author upon reasonable request.

Code availability (software application or custom code)

Not applicable

Authors' contributions

W. W and D.H carried out the animal model design and carried out the molecular study. P.Z, K.L and S.W participated in the data analysis. J.W and L.C conceived of the study, and participated in its design and coordination and helped to draft the manuscript. All authors read and approved the final manuscript and they all declare that no competing interests exist.

References

1. Sofroniew, M.V., *Dissecting spinal cord regeneration.* Nature, 2018. **557**(7705): p. 343-350.
2. Schwab, J.M., et al., *Raising awareness for spinal cord injury research.* Lancet Neurol, 2018. **17**(7): p. 581-582.
3. Tran, A.P., P.M. Warren, and J. Silver, *The Biology of Regeneration Failure and Success After Spinal Cord Injury.* Physiol Rev, 2018. **98**(2): p. 881-917.
4. Cristante, A.F., et al., *Therapeutic approaches for spinal cord injury.* Clinics (Sao Paulo), 2012. **67**(10): p. 1219-24.
5. Griffin, J.M. and F. Bradke, *Therapeutic repair for spinal cord injury: combinatory approaches to address a multifaceted problem.* EMBO Mol Med, 2020. **12**(3): p. e11505.
6. Devivo, M.J., *Epidemiology of traumatic spinal cord injury: trends and future implications.* Spinal Cord, 2012. **50**(5): p. 365-72.
7. Yao, W., et al., *The CDR1as/miR-7/TGFBR2 Axis Modulates EMT in Silica-Induced Pulmonary Fibrosis.* Toxicol Sci, 2018. **166**(2): p. 465-478.
8. Dias, D.O., et al., *Reducing Pericyte-Derived Scarring Promotes Recovery after Spinal Cord Injury.* Cell, 2018. **173**(1): p. 153-165 e22.
9. Liu, R., et al., *microRNA-21 regulates astrocytic reaction post-acute phase of spinal cord injury through modulating TGF-beta signaling.* Aging (Albany NY), 2018. **10**(6): p. 1474-1488.
10. Hara, M., et al., *Interaction of reactive astrocytes with type I collagen induces astrocytic scar formation through the integrin-N-cadherin pathway after spinal cord injury.* Nat Med, 2017. **23**(7): p. 818-828.
11. Anderson, M.A., et al., *Astrocyte scar formation aids central nervous system axon regeneration.* Nature, 2016. **532**(7598): p. 195-200.
12. Chen, W. and E. Schuman, *Circular RNAs in Brain and Other Tissues: A Functional Enigma.* Trends Neurosci, 2016. **39**(9): p. 597-604.
13. van Rossum, D., B.M. Verheijen, and R.J. Pasterkamp, *Circular RNAs: Novel Regulators of Neuronal Development.* Front Mol Neurosci, 2016. **9**: p. 74.

14. Li, T.R., et al., *Circular RNA: a new star in neurological diseases.* Int J Neurosci, 2017. **127**(8): p. 726-734.
15. Qu, S., et al., *Circular RNA: A new star of noncoding RNAs.* Cancer Lett, 2015. **365**(2): p. 141-8.
16. Wang, W., et al., *Identification of noncoding RNA expression profiles and regulatory interaction networks following traumatic spinal cord injury by sequence analysis.* Aging (Albany NY), 2019. **11**(8): p. 2352-2368.
17. Kim, D., et al., *TopHat2: accurate alignment of transcriptomes in the presence of insertions, deletions and gene fusions.* Genome Biol, 2013. **14**(4): p. R36.
18. Zhang, X.O., et al., *Complementary sequence-mediated exon circularization.* Cell, 2014. **159**(1): p. 134-147.
19. Kanehisa, M., et al., *KEGG: new perspectives on genomes, pathways, diseases and drugs.* Nucleic Acids Res, 2017. **45**(D1): p. D353-D361.
20. Wang, W., et al., *MicroRNA-21a-5p promotes fibrosis in spinal fibroblasts after mechanical trauma.* Exp Cell Res, 2018. **370**(1): p. 24-30.
21. Wang, W., et al., *MicroRNA-21-5p mediates TGF-beta-regulated fibrogenic activation of spinal fibroblasts and the formation of fibrotic scars after spinal cord injury.* Int J Biol Sci, 2018. **14**(2): p. 178-188.
22. Hawasli, A.H., et al., *Spinal Cord Injury Disrupts Resting-State Networks in the Human Brain.* J Neurotrauma, 2018. **35**(6): p. 864-873.
23. Agarwal, V., et al., *Predicting effective microRNA target sites in mammalian mRNAs.* Elife, 2015. **4**.
24. Berindan-Neagoe, I., et al., *MicroRNAome genome: a treasure for cancer diagnosis and therapy.* CA Cancer J Clin, 2014. **64**(5): p. 311-36.
25. Rybak-Wolf, A., et al., *Circular RNAs in the Mammalian Brain Are Highly Abundant, Conserved, and Dynamically Expressed.* Mol Cell, 2015. **58**(5): p. 870-85.
26. Geng, H.H., et al., *The Circular RNA Cdr1as Promotes Myocardial Infarction by Mediating the Regulation of miR-7a on Its Target Genes Expression.* PLoS One, 2016. **11**(3): p. e0151753.
27. Hansen, T.B., et al., *miRNA-dependent gene silencing involving Ago2-mediated cleavage of a circular antisense RNA.* EMBO J, 2011. **30**(21): p. 4414-22.
28. Memczak, S., et al., *Circular RNAs are a large class of animal RNAs with regulatory potency.* Nature, 2013. **495**(7441): p. 333-8.
29. Hansen, T.B., et al., *Natural RNA circles function as efficient microRNA sponges.* Nature, 2013. **495**(7441): p. 384-8.
30. Li, X., et al., *Circular RNA CDR1as regulates osteoblastic differentiation of periodontal ligament stem cells via the miR-7/GDF5/SMAD and p38 MAPK signaling pathway.* Stem Cell Res Ther, 2018. **9**(1): p. 232.
31. Junn, E., et al., *Repression of alpha-synuclein expression and toxicity by microRNA-7.* Proc Natl Acad Sci U S A, 2009. **106**(31): p. 13052-7.

32. Karran, E., M. Mercken, and B. De Strooper, *The amyloid cascade hypothesis for Alzheimer's disease: an appraisal for the development of therapeutics.* Nat Rev Drug Discov, 2011. **10**(9): p. 698-712.
33. Zhou, X., et al., *Role of the ciRS-7/miR-7 axis in the regulation of proliferation, apoptosis and inflammation of chondrocytes induced by IL-1beta.* Int Immunopharmacol, 2019. **71**: p. 233-240.
34. Zheng, Q., et al., *Circular RNA profiling reveals an abundant circHIPK3 that regulates cell growth by sponging multiple miRNAs.* Nat Commun, 2016. **7**: p. 11215.
35. Chen, H., et al., *Circular RNA CDR1as acts as a sponge of miR-135b-5p to suppress ovarian cancer progression.* Onco Targets Ther, 2019. **12**: p. 3869-3879.
36. Zhang, Z., T. Yang, and J. Xiao, *Circular RNAs: Promising Biomarkers for Human Diseases.* EBioMedicine, 2018.
37. Okuda, H., et al., *miR-7 suppresses brain metastasis of breast cancer stem-like cells by modulating KLF4.* Cancer Res, 2013. **73**(4): p. 1434-44.

Figures

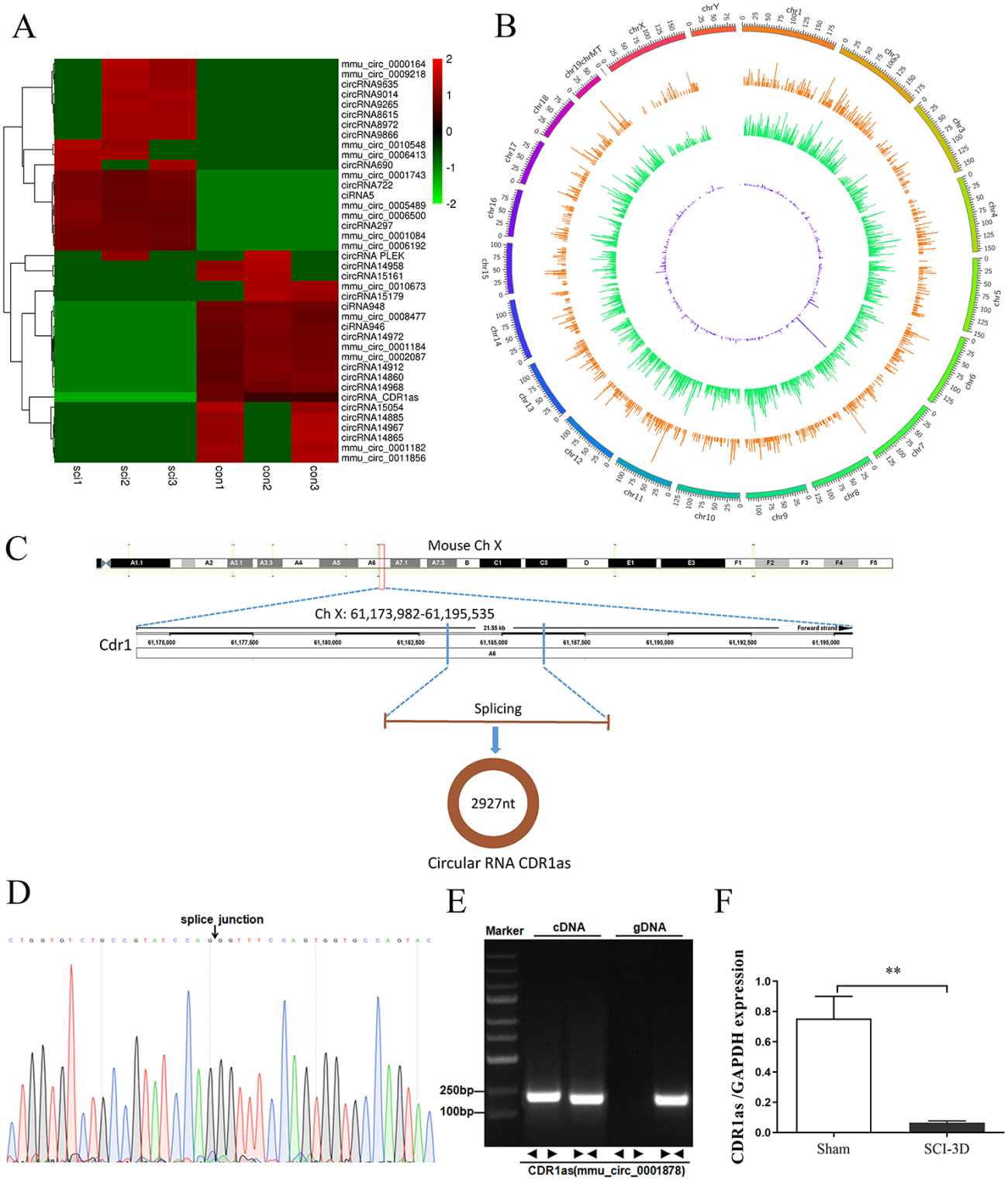

Figure 1

CircRNA expression profiles and validation of CDR1as Hierarchical clustering of circRNA expression. circRNAs are shown in the right-hand column. Red pixels correspond to an increased abundance of the gene in the indicated sample, whereas green pixels indicate a decrease, $p < 0.05$ (A). The distribution of circRNAs along each chromosome, $p < 0.05$ (B). A schematic diagram indicates the genomic loci of the CDR1as gene and CDR1as (C). Sequencing results of divergent PCR products generated from CDR1as

confirmed the head-to-tail junction point (D). Convergent or divergent primers were used to validate the existence of circCDR1as in mouse spinal cord via RT-PCR. circRNA could be amplified by convergent primers in both cDNA and gDNA and amplified by divergent primers in cDNA without gDNA. The direction of black triangles represents divergent and convergent primers (E). The relative expression of CDR1as was measured in the lesion epicentre of spinal tissues on day 3 post-SCI via qRT-PCR (F). Data are expressed as the mean ± standard deviation. **p < 0.01, ***p < 0.001.

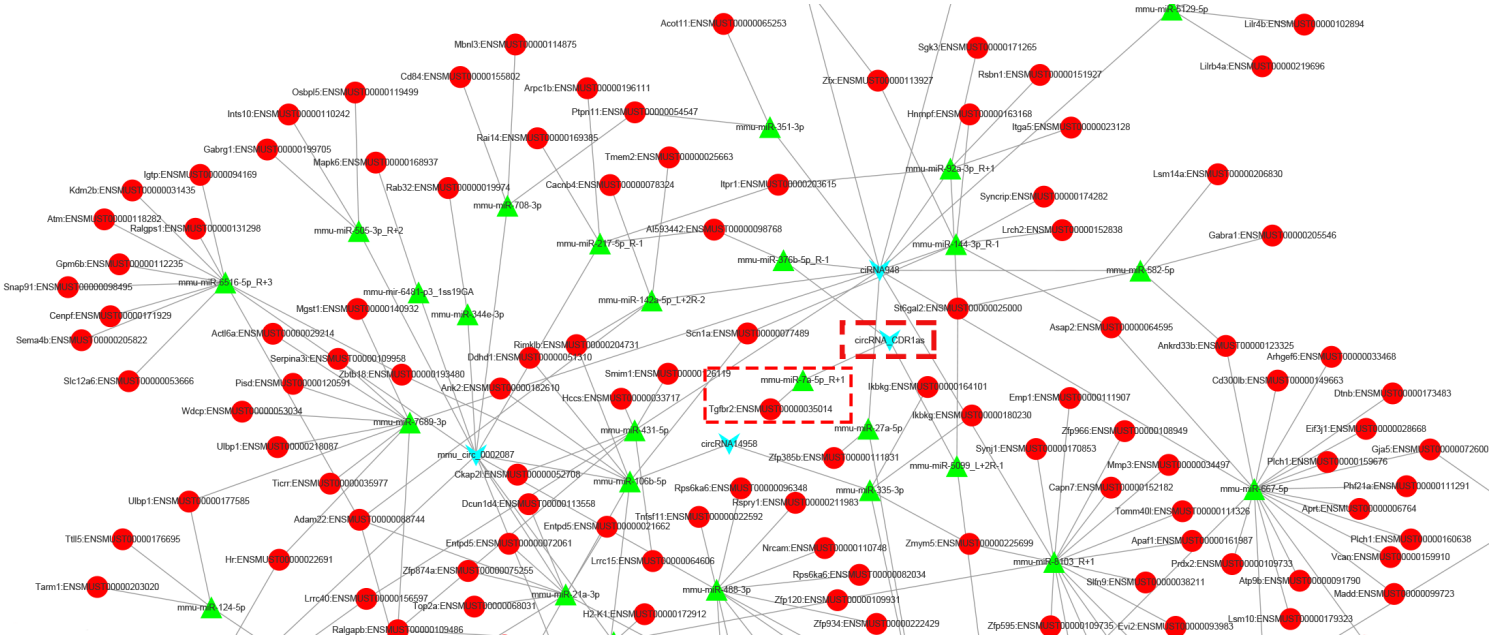

Figure 2

CircRNA/miRNA/mRNA network analysis. The CDR1as/miR-7a-5p/TGF-βR2 axis was predicted and constructed (outlined in red).

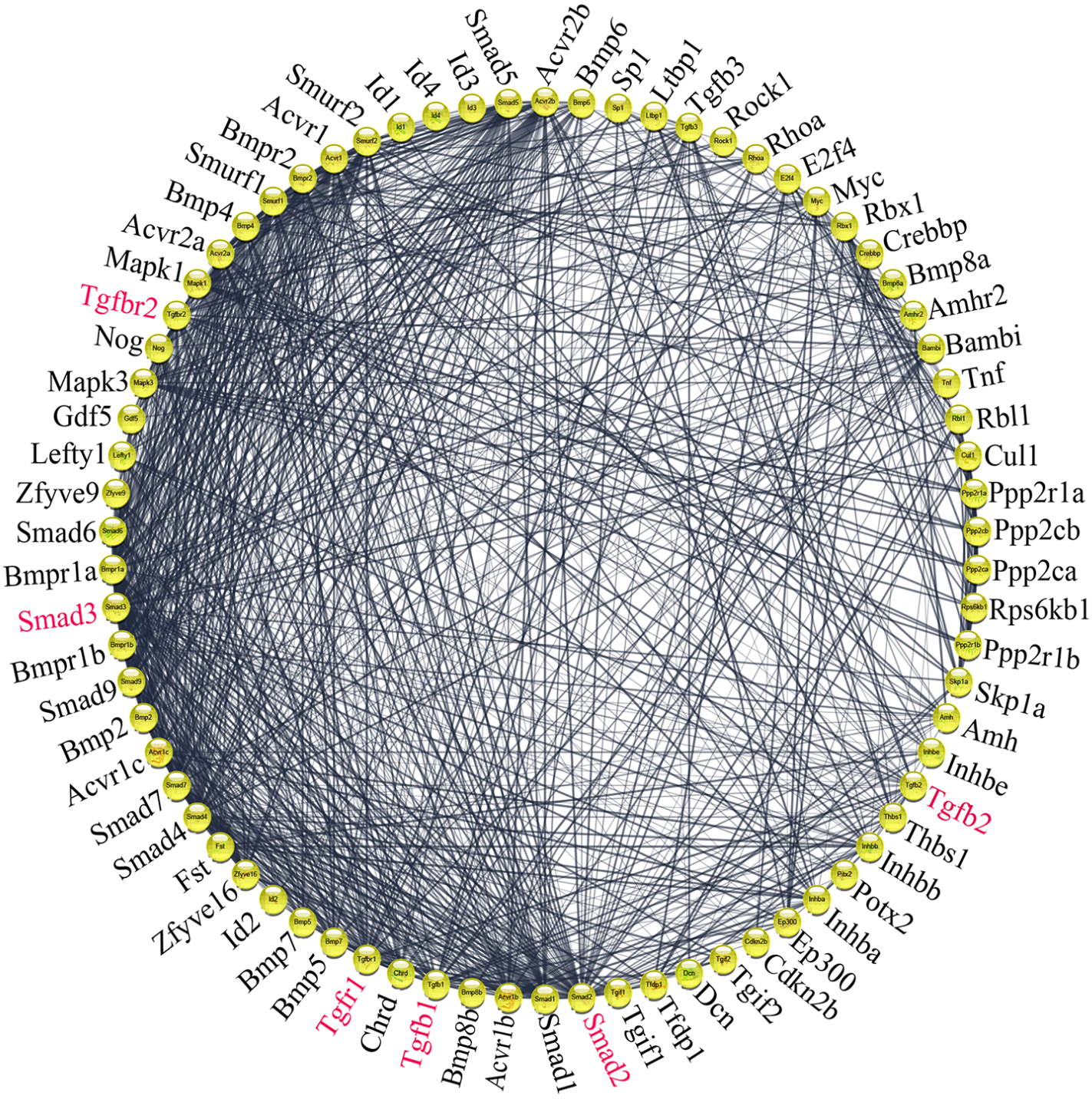

Figure 3

Stringtie enrichment of the differentially expressed Smads signalling pathway related proteins after SCI.

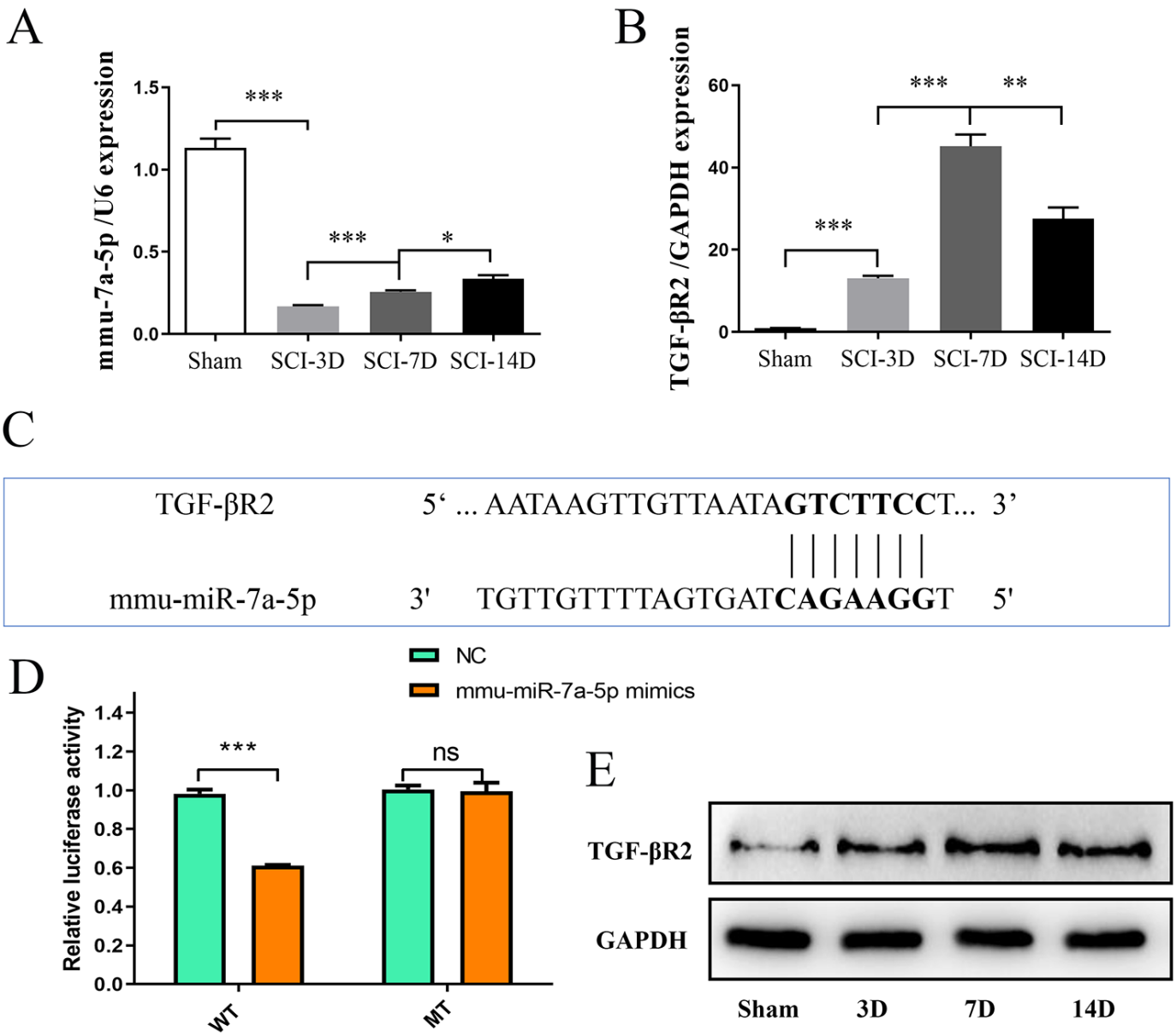

Figure 4

Validation of the targeted relationship between miR-7a-5p and TGF-βR2. qRT-PCR revealed the miR-7a-5p (A) and TGF-βR2 (B) level in the lesion epicentre of spinal tissues by qRT-PCR on days 3,7,and 14 post-SCI. A predicted miR-7a-5p target site in the 3'UTR of TGF-βR2(C). Relative luciferase expression of wild-type and mutant TGF-βR2 UTR-bearing luciferase vectors, co-transfected with miR-7a-5p expression vectors (D). Western Blot shows the level of TGF-βR2 protein in the epicentre of spinal tissues on days 3,7, and 14 post-SCI (E). Data are expressed as the mean ± standard deviation. **P<0.01, ***P<0.001.

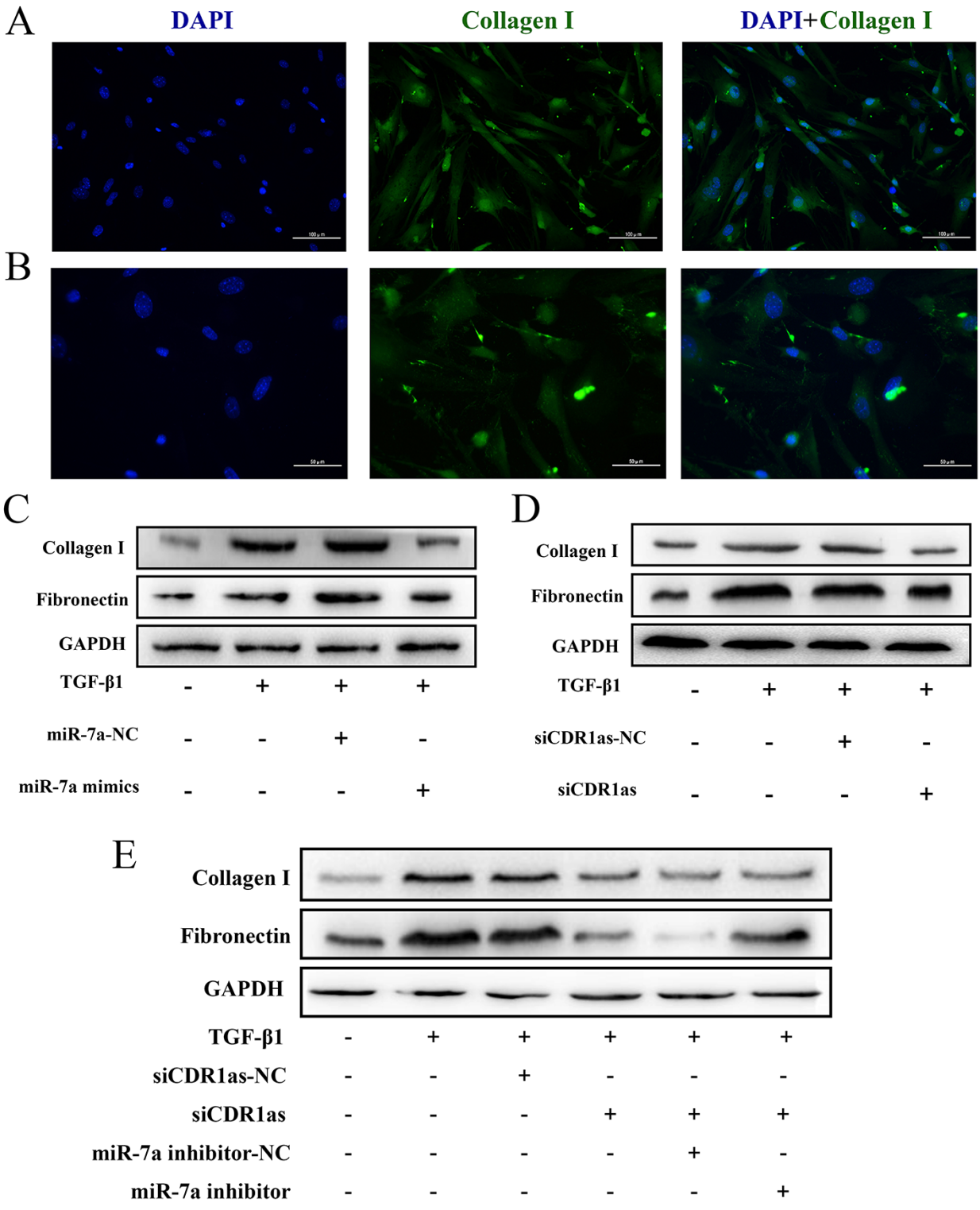

Figure 5

CDR1as/miR-7a-5p /TGF-βR2 axis regulated spinal fibroblast fibrosis. Primary spinal cord fibroblasts were identified by immunofluorescence assays. The nucleus is stained blue by DAPI. Collagen I was identified by green fluorescence. The plots below (B, bar= 100 μm) are partial magnifications of the plots above (A, bar= 50 μm). The relative expression levels of fibronectin and collagen I protein in the control, TGF-β1, TGF-β1+ miR-7a-5p mimic NC, and TGF-β1+ miR-7a-5p mimics groups was measured in spinal

fibroblasts by Western Blot (C). The relative expression levels of fibronectin and collagen I protein in the control, TGF-β1, TGF-β1+ siCDR1as NC, and TGF-β1+ siCDR1as groups was measured in spinal fibroblasts by Western Blot (D). Fibronectin and Collagen I protein levels were detected by Western Blot after co-transfection with siCDR1as + miR-7a-5p inhibitor, or their negative control, in spinal fibroblasts, with or without TGF-β1 (E).

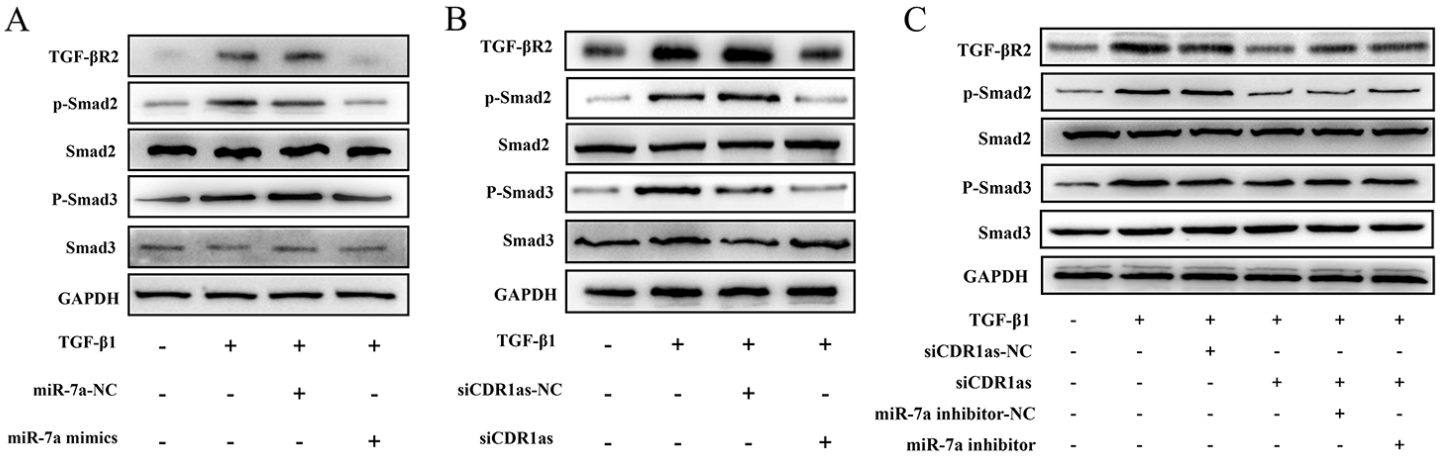

Figure 6

CDR1as/miR-7a-5p /TGF-βR2 axis affects the activation of Smads signaling pathway. The relative expression levels of Smad2, phospo-Smad2, Smad3, and phospo-Smad3 in spinal fibroblasts transfected with miR-7a-5p mimics/NC with or without TGF-β1assessed via Western Blot (A). The relative expression levels of Smad2, phospo-Smad2, Smad3, and phospo-Smad3 in spinal fibroblasts transfected with siCDR1as /NC with or without TGF-β1 assessed via Western Blot (B). After co-transfection with siCDR1as and miR-7a-5p inhibitor in spinal fibroblasts with or without TGF-β1, Smad2, phospo-Smad2, Smad3, and phospo-Smad3 protein levels were measured by Western Blot (C).

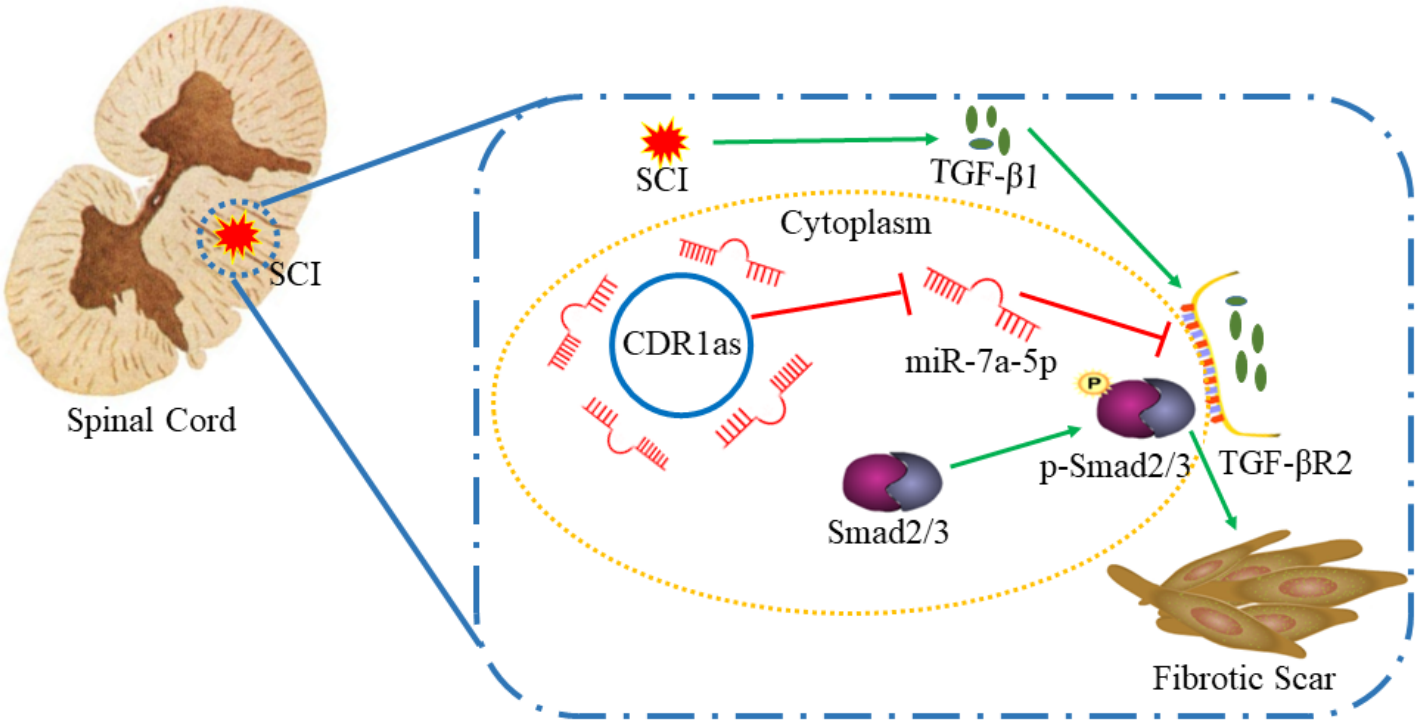

Figure 7

CDR1as regulates spinal fibrosis through the miR-7a-5p /TGF-βR2 axis.

Supplementary Files

This is a list of supplementary files associated with this preprint. Click to download.

- figureS1.pdf